



Final Report for MEng Project

Development of MRI T2* Mapping Model for N-Periodic ka-SPGR Sequence: A Promising Technique for Parkinson's Disease Biomarker Detection

Author name: Yifei Jin
Supervisor: Dr. Neal K. Bangerter

Submitted in partial fulfilment of the requirements for the award of MEng in Biomedical Engineering from
Imperial College London

Thursday, 15 June 2023 Word count: 4084

Contents

1 Abstract	3
2 Introduction	4
3 Theory	6
3.1 Multi-echo GRE	6
3.2 N-periodic ka-SPGR	7
4 Methods	8
4.1 Model Simulation and analysis	8
4.1.1 Simulation setup	8
4.1.2 Data simulation	9
4.1.3 Analysis method	10
4.2 MRI data acquisition and analysis	10
4.2.1 MRI scan setup	10
4.2.2 Image processing	11
4.2.3 Analysis method	12
5 Results	13
5.1 Model simulation result	13
5.1.1 Optimal ka-SPGR parameter	13
5.1.2 Optimal ka-SPGR accuracy and precision	14
5.2 Phantom MRI scan results	14
5.2.1 Quantitative T2* mapping image	14
5.2.2 Percentage bias	15
5.2.3 Effective T2* Signal-to-Noise ratio	16
6 Discussion and Conclusion	17
7 Acknowledgements	19
References	20

1 Abstract

Early diagnosis and tracking of Parkinson's disease can be achieved by detecting Substantia Nigra iron overloaded with MRI relaxometry parameter T2*, unfortunately, accurate high-resolution T2* mapping result is difficult to achieve at the brain stem due to tissue motion. A novel technique N-periodic ka-SPGR is proposed to be motion robust and can be used to generate quantitative T2* mapping images, while neither analysis of the techniques' T2* mapping performance nor optimised scan parameters were suggested. This study provides optimised parameters (period and repetition time) of ka-SPGR specifically for PD biomarker detection based on computer simulation. It is followed by a phantom scanning experiment with the optimised ka-SPGR sequences and the T2* mapping result using Multi-echo GRE is used as Gold-standard to compare with. 7-periodic or 12-periodic ka-SPGR with a repetition time of 6ms is suggested to optimise the performance. The 12-periodic ka-SPGR is more robust to noise, while the 7-periodic provides better efficiency. The accuracy and precision of both sequences are proven by analysing simulation and phantom experiment results, which both show a percentage bias $< \pm 10\%$. However, the study is limited by the phantom's alignment with the substantia nigra and can be improved using a phantom specifically adjust for substantia nigra tissue property. Additionally, to further prove the reliability of ka-SPGR for PD biomarker detection, massive in-vivo experiments are desirable to evaluate its performance in realistic and complex environments.

2 Introduction

Parkinson's disease (PD) is a chronic neurodegenerative disease that affects the motor region of the brain and causes tremors, it is the second most common neurodegenerative disorder and approximately 9.4 million people suffer from PD worldwide [19, 16]. The disease's pathophysiology is irreversible and currently has no cure. Therefore, early detection and accurate progress tracking are essential for supporting PD treatment and new solution development, which can be achieved by having effective biomarkers. One of the PD's early signs is iron overloaded at the substantia nigra (SN) region in the brain stem, as shown in Figure 1 [6, 15, 3], which can be detected using Magnetic Resonance Imaging (MRI) technique [2, 13].

MRI is a non-invasive medical imaging technique. It constructs images based on the proton's signal responses to a train of radiofrequency excitations (pulse sequence) under different chemical environments. The MRI signal decay exponentially with the time constant $T2^*$, which is tissue and magnetic field inhomogeneity dependent. As the overloaded iron caused by PD distorts the magnetic field, a more rapid decay of the MRI signal and a smaller $T2^*$ value will be observed at the SN, various studies have shown this change of $T2^*$ value can be used as an effective biomarker for PD [3, 15]. A traditional way of generating quantitative $T2^*$ images is to acquire MR images at different times and fit the signal's exponential decay in each voxel to get the $T2^*$, this technique is known as $T2^*$ mapping using Multi-Echo Gradient Echo (GRE) sequence [5]. However, the complex tissue movement at the brain stem, which is related to blood flow, central cerebellum fluid flow, and the cardiac cycle, results in tissue motion artefacts on MR images and makes high-quality brain stem MRI difficult to achieve [20, 11]. Additionally, it makes getting an accurate $T2^*$ image of the brain even more difficult as one $T2^*$ image is constructed based on multiple high-quality MR images.

A simple way to reduce the effect of tissue motion is acquiring multiple MR images and averaging to reduce motion artefacts, but it will lengthen the acquisition time. Using a larger voxel size can also reduce the impact of the tissue movement, however, high-resolution MR images are essential to capture important tissue information in the tiny millimetre-size SN region [20]. Other post-processing-based methods can perform motion correction on the acquired images, but these techniques mostly focus on the whole-body movement instead of the tissue motion [14].

Based on all these limitations, a new $T2^*$ imaging technique is suggested [12], which can reduce the impact of motion while maintaining short acquisition time and good resolution, using the MRI pulse sequence named k-space-aliased Spoiled Gradient-Recalled (ka-SPGR). The images acquired with ka-SPGR are not simply related by decay time, instead, each image contains information coming from different times of the $T2^*$ decay. By extracting useful information from each acquired image and summing it up, the $T2^*$ related signal decay at specific times can be reconstructed and $T2^*$ can be calculated by fitting the exponential decay. Theoretically, even if the movement of the brain creates artefacts in some acquisition, it will not have a huge impact on the reconstructed $T2^*$ decay signal, as the signal is obtained by averaging across multiple acquisitions. However, there was no quantitative analysis of the ka-SPGR $T2^*$ measurement accuracy, and no suggested optimal

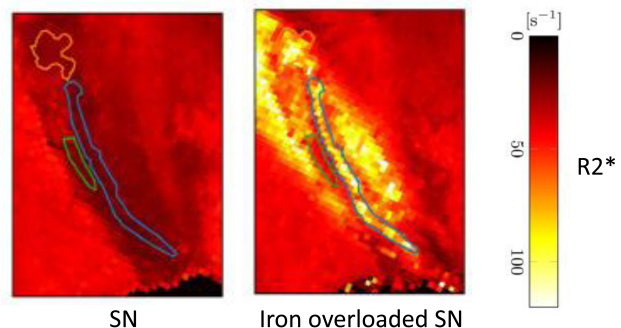


Figure 1: The iron overloaded at the substantia nigra can be detected using MRI technique $R2^*$ mapping, where $R2^*$ equals $\frac{1}{T2^*}$. (Brammerloh, Malte et al., 2021)

MRI scanning parameters for the ka-SPGR sequence. Therefore, evaluating the ka-SPGR's T2* accuracy and obtaining optimal parameters is desirable, before proving the motion robustness of the ka-SPGR technique in vivo.

The aim and objectives of this project are the following:

1. Model the ka-SPGR T2* measurement based on Bloch simulation, followed by Monte Carlo tests to analyse the bias and variation of the measured T2* when acquisition noise is considered.
2. Suggest optimal scan parameters based on analysis of the simulation results.
3. Acquire MRI data from a phantom using the gold-standard technique (Multi-echo GRE) and ka-SPGR with optimised parameters.
4. Compare the reconstructed quantitative T2* mapping images of the gold-standard technique and ka-SPGR.
5. Compute the T2* percentage error and T2* effective signal-to-noise ratio of the acquired data to evaluate the practical performance of ka-SPGR and compare it with the gold-standard technique.

3 Theory

In MRI, a train of radiofrequency (RF) pulse sequences excites the magnetised spins to generate the MRI signal. During excitation, the magnetisation initially aligned with the main magnetic field in the longitudinal direction is tipped towards the transverse plane with a longitudinal flip of α° and a transverse phase shift ϕ . After the excitation, the magnetisation relaxes with a longitudinal ~~regrow~~ with the time constant T1 and a transverse decay. The transverse component of magnetisation is measured to form an MR image and the signal will decay with a time constant T2 or T2* depending on the MRI pulse sequence used. The time between excitation and acquisition of the signal is known as echo time (TE), and the time between adjacent excitations is repetition time (TR). The MRI signal is acquired in Fourier ~~transform~~ space, known as k-space, and the resulting image is reconstructed by performing the inverse Fourier transform of the acquired k-space. The two types of MRI pulse sequences used in this project are briefly introduced below. [18]

3.1 Multi-echo GRE

Using a ~~gradient echo (GRE)~~ based pulse sequence, the acquired MR signal ~~decay~~ with the time constant T2* [4]. The gold-standard T2* measuring technique – Multi-echo ~~GRE~~ is performed by measuring the MR signal at multiple TEs in one TR with ~~GRE~~ sequence and fitting monoexponential decay to get the time constant T2* voxel by voxel as shown in Figure 2.

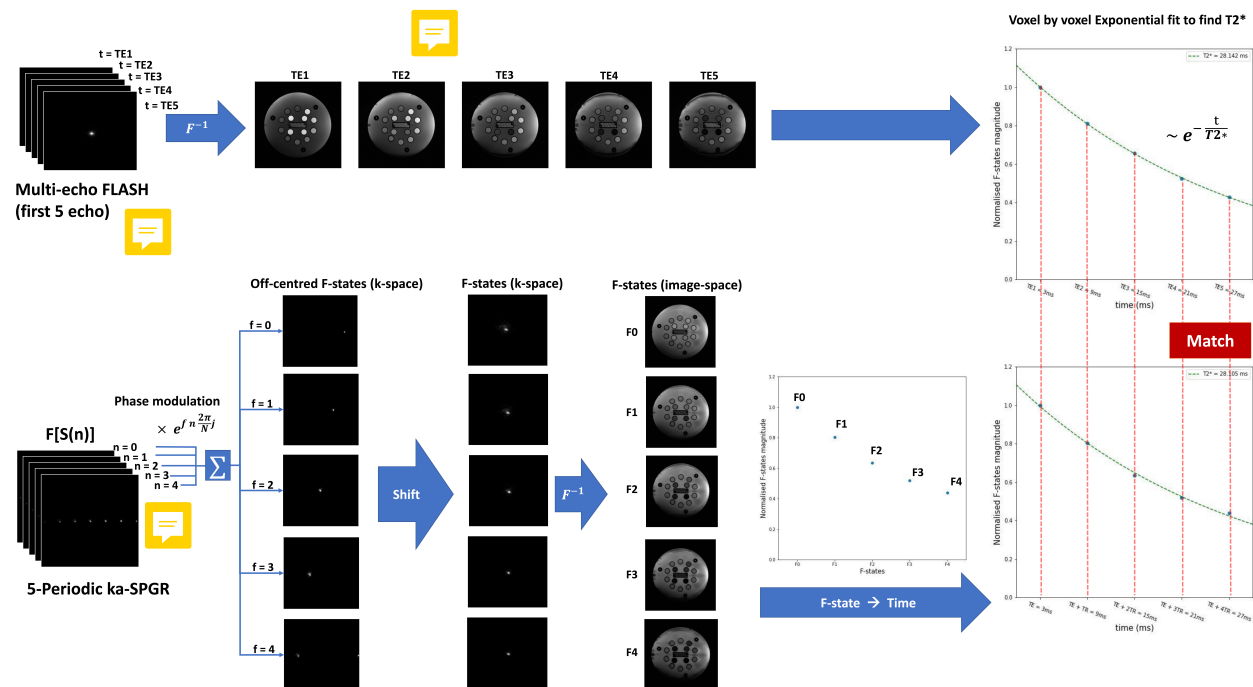


Figure 2: Flow chart of Multi-echo GRE and N-periodic ka-SPGR image formation and T2* calculation process.

Starting from the raw k-space data acquired by the MRI scanner (left) to the voxel-by-voxel exponential fit for T2* value calculation (right). K-spaces and images of 5-echo ~~GRE~~ and 5-Periodic ka-SPGR are used to aid illustration. The matching of the two techniques for comparison purposes, which will be discussed in the Method section, is shown in the exponential fitting figures on the right.

3.2 N-periodic ka-SPGR

The N-periodic ka-SPGR sequence is based on short TR fast GRE [7] with TE = TR/2, which yields a steady-state behaviour of the signal. Additionally, quadratic radiofrequency-spoiling (RF-spoiling) and gradient-spoiling are applied for the N-periodic ka-SPGR sequence. RF-spoiling is applied by constantly exciting the spins with a quadratic phase cycling given by the function below [7, 12],

$$\phi_n = 0.5 \times n^2 \times \frac{2\pi}{N}, (n = 0, 1, 2\dots). \quad (1)$$

, and the k-spaces of acquired S(n)s are shown at the bottom left figure in Figure 2. By adding RF-spoiling, N different and periodically repeating steady-state signals S(n) are yielded, each signal is the summation of the T2* related decay signals at certain times weighted by corresponding phase modulation, which is shown by the analytical solution below [12],

$$S(n) = e^{j\omega TE} \sum_F A e^{-(TE+F \times TR)/T_2^*} e^{jF\omega TR} e^{jnF \frac{2\pi}{N}}. \quad (2)$$

The T2* related component in the equation, $A e^{-(TE+F \times TR)/T_2^*}$, is known as the configuration state or F-state signal and is denoted as F_0 if F in the equation equals 0. Furthermore, gradient spoiling is added to shift and split the F-states away from the centre of the k-space by different amounts, as shown in the bottom left image of Figure 2, which shows the acquired image with 5 F-states shifting away from the centre.

The k-space of each F-state can be reconstructed by summing up N-acquired signals with corresponding phase modulation followed by shifting the k-space back to the centre. An inverse Fourier transform is then performed to generate the F-states images, which are then used to fit T2*. An illustration of this procedure using 5-periodic ka-SPGR is provided in Figure 2.

4 Methods

4.1 Model Simulation and analysis

A Python-based computer simulation is built to model the ka-SPGR T2* mapping performance when different TR and **periods** are used. The simulated results are then used to find the optimal ka-SPGR parameters for PD biomarker detection. The full version of the Python code for simulation, image reconstruction and analysis can be found in the following GitHub repository: https://github.com/Yifei-Jin/Final_Year_Project.git

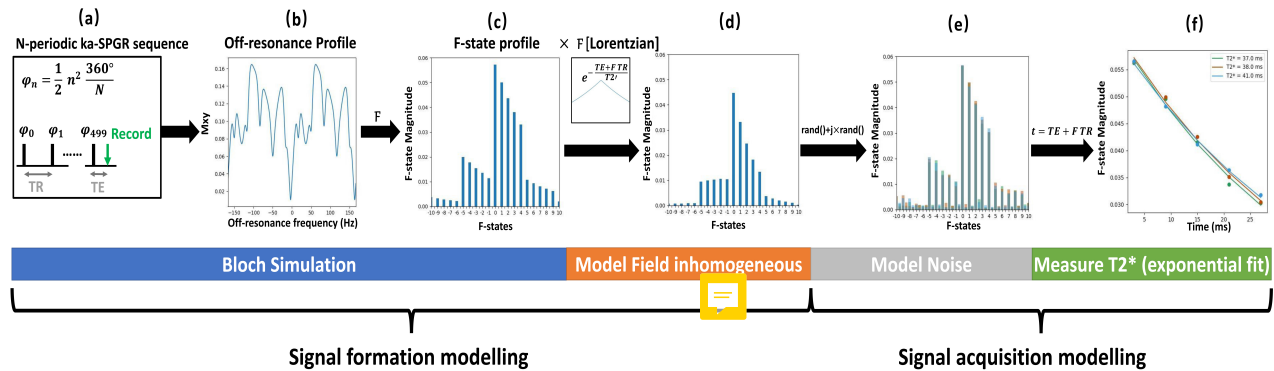


Figure 3: ka-SPGR computer simulation flow chart

4.1.1 Simulation setup

As shown in Figure 3, the computer simulation can be described in 2 sections - signal formation modelling, where the ideal Bloch simulation is performed followed by applying the magnetic field **inhomogeneous effects**; and acquisition modelling, where the noise is considered and T2* fitting is performed.

- Bloch Simulation

Using the well known Bloch equation [18], the performance of the spin with specific tissue properties (T1, T2) under different applied pulse sequences can be modelled by applying specific α , ϕ , TR and TE. As the project focused on SN region T2* mapping, SN's T1 (800ms) and T2 (44ms) are used in the computer

Simulation Parameters	T2	44 ms
T1	800 ms	
Number of different off-resonance frequencies	1000	
Flip angle, α	10	
Initial magnetisation, M0	1	
Number of TR before record signal	500	
Sample size	1000	
Data simulation range	N	3~12
TR range	2~10ms (0.4 ms increment)	
T2* range	13~53 ms (1 ms increment)	

Table 1: Computer simulation parameters and range

simulation model, suggested by previous research on SN [17, 3]. A 10° optimal flip angle calculated from the Ernst equation is used [8], and RF-spoiling is applied by implementing phase shift ϕ based on equation (1). Additionally, to ensure the steady state is fully reached, the spin is repeatedly excited 500 times before acquiring the signal. The structure of the pulse sequence is shown in the left first figure in Figure 3, and the parameters used are summarised in Table 1. An off-resonance profile is then generated, as shown in Figure 3 (b), which models the performance of spins under external disturbances by simulating spins with different extra phase shifts, and the Fourier transform of the off-resonance profile is equal to the configuration F-states, as shown in Figure 3 (c) [22].

- Magnetic field inhomogeneity modelling

The field inhomogeneous effect caused by iron overload in the tissue can be modelled by convolving the Lorentzian distributed field **inhomogeneous** with the off-resonance profile [23]. With a selected ground truth T2* and the known SN T2, the inhomogeneous effect related to the ground truth T2* can be calculated using the relationship [4],

$$\frac{1}{T2^*} = \frac{1}{T2} + \gamma \Delta B_{inhomogeneous} \quad (3)$$

and applied to the Bloch simulation model. However, as shown in Figure 3 (d), in this computer simulation, multiplying the F-states signal with the Fourier transform of Lorentzian - an exponential curve with the time constant $T2' = \frac{1}{\gamma \Delta B_{inhomogeneous}}$ is performed instead of the complicated convolution, as it is an equivalent operation supported by the property of Fourier transforms.

- Noise modelling

In reality, an MRI scanner introduces noise while acquiring the signal [10]. For ka-SPGR with different periods and TR, the acquisition noise is modelled using zero-mean Gaussian with standard deviation equals $\frac{F_0}{\sqrt{N}} \times 5\%$, where the F_0 is the F-state magnitude simulated when T2* = 33ms, the mean of PD and healthy SN T2*. Then the generated Gaussian noises are added to the imaginary and real parts of the simulated F-states signal. Figure 3 (e) shows 3 times of F-state acquisition modelling, each different colour indicates one sample acquisition. Additionally, in the data simulation, 1000 acquisitions are made to perform the Monte Carlo experiment and analyse the performance.

- T2* measurement modelling

To model the T2* calculation of N-periodic ka-SPGR, the exponential fit should only use the first N F-state magnitude $F_0 \dots F_{N-1}$, because only these F-states can be reconstructed from the acquired signal using N-periodic ka-SPGR. As shown in Figure 3 (f), only the first 5 F-states are used to fit the exponential for 5-periodic ka-SPGR.

4.1.2 Data simulation

The data is simulated for spins with ground truth T2* of 13-53ms when applying 3 - 12 periodic ka-SPGR sequences with different TRs from 2ms to 10ms. The bottom section of Table 1 summarised the scan parameters covered by the data simulation. The range of ground truth T2* is selected specifically for analysing PD biomarker detection accuracy, which is between the PD patients' (13ms) and healthy SN T2* (53ms) [3]. The above periodicity and TR ranges are selected for the simulation because a periodicity less than 3 is not able to provide enough data points for fitting the exponential curve, and a TR smaller than 2ms **can't** be achieved by a  scanner, also, periodicity greater than 12 or TR greater than 10ms both leads to an unacceptable long acquisition time.

On top of the selected range, Monte Carlo experiments are performed and by fitting each group of acquired

F-states, 1000 measured $T2^*$ can be obtained for each ground truth $T2^*$ value for different periodic ka-SPGR with different TR.

4.1.3 Analysis method

The simulated $T2^*$ are then further analysed using percentage bias and standard deviation to find optimal scan parameters. The percentage bias of the simulated $T2^*$ shows the accuracy of the $T2^*$ measurement and it ~~hugely~~ depends on the choice of period and TR. As shown in Figure 3, the ~~x-coordinate~~ of points used for exponential fit is $TE + F \times TR, F = 0 \dots (N - 1)$, by using different periods and TRs, different parts and ranges of the exponential curve is sampled, which will affect the accuracy of the exponential fit. By locating the minimum average percentage bias, the optimal period and TR for ka-SPGR that maximises $T2^*$ measurement accuracy can be found. The standard deviation of the measured $T2^*$ using the optimised parameter is then computed to evaluate the variation of the measurement and verify the reliability of the technique. According to [3] the iron-induced change in SN $T2^*$ is $40ms \pm 6.5ms$, which has a 16% percentage error, to detect the change, a $T2^*$ percentage error $<5\%$ would be acceptable. Once the accuracy and precision of the chosen parameter are proven, it is then used for the MRI phantom scanning experiment.

4.2 MRI data acquisition and analysis

 MRI scan using ka-SPGR sequence with optimised scan parameter ~~is~~ performed on a phantom. The $T2^*$ values ~~are~~ calculated and compared with the ground truth $T2^*$ value obtained using the gold-standard Multi-echo ~~GRE~~ technique. Followed by a comparison between the ka-SPGR and the Multi-echo ~~GRE~~ techniques with ~~controlled variables~~.

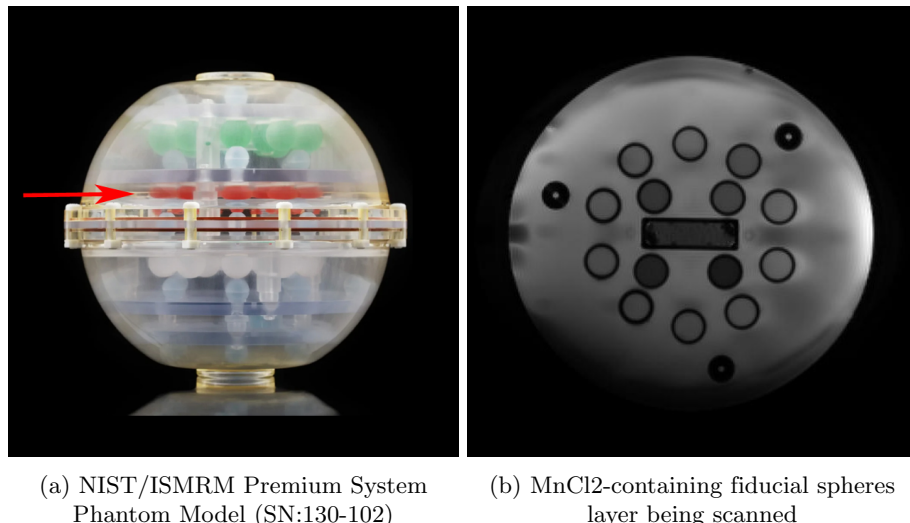


Figure 4: The phantom used for the scanning experiment.
The red arrow in (a) shows the MnCl₂-containing layer where the scan is performed

4.2.1 MRI scan setup

NIST/ISMRM Premium System Phantom Model (SN:130-102) shown in Figure 4a is used as the scanning object, and a slice acquisition is performed at the MnCl₂-containing fiducial spheres layer (Figure 4b).  Multi-echo FLASH (Siemens, 3T), one commonly used Multi-echo ~~GRE~~ sequence, ~~is~~ used as the gold standard $T2^*$ measuring technique to obtain the ground truth $T2^*$ value for each fiducial sphere.

MRI signals ~~are~~ acquired from the phantom using 7 and 12-periodic ka-SPGR sequences with TR = 6ms and 10° flip angle, which ~~are~~ optimised from the computer simulation. The ~~middle F-state~~ and amount of gradient

spoiler shift ~~are~~ carefully selected (Table 2b) to make sure the required N F-states are separated while still within the k-space acquisition range.

MRI signals are also acquired using Multi-echo FLASH with parameters chosen to match with ka-SPGR. In order to minimise the influence of the exponential fitting efficiency, the number and position of data points used to fit the exponential curve ~~should be~~ consistent for the two techniques. Therefore, to achieve the match shown in Figure 2, the Multi-echo FLASH TEs start with ka-SPGR's TE and following by an increment equal to ka-SPGR's TR as shown in Table 2a. Additionally, the number is kept consistent by using the first N acquisition of Multi-echo FLASH to fit exponential fit when compare with N-periodic ka-SPGR. Also, the image and voxel sizes are matched for all scanning performed, as shown in Table 2.

A 90° flip angle FLASH is used to obtain an accurate T2* ground truth value for evaluating ka-SPGR T2* accuracy, and a 20° flip angle FLASH is used to match with ka-SPGR's low flip angle aiming at comparing the 2 techniques' efficiency under similar ~~environment~~.

Image size	256×256	
Voxel size	1.0mm×1.0mm×5.0 mm	
TR	100 ms	
TE	3 ~ 69 ms (6ms increment)	
Flip angle	20°	90°
Number of echo	12	12
Effective scan time	26 s	26 s

(a) Multi-echo GRE parameters

Image size	256×256			
Voxel size	1.0mm×1.0mm×5.0 mm			
TR	6 ms			
TE	3 ms			
Flip angle	10°			
N (Number of echo = N)	5	6	7	12
Middle F-state	F2	F2	F3	F5
Gradient spoiler shift	40 lines	40 lines	34 lines	20 lines
Effective scan time (Exclude dummy scan)	8 s	9 s	11 s	18 s

(b) ka-SPGR parameters

Table 2: Scanning parameters for pulse sequences

4.2.2 Image processing

The F-states images of ka-SPGR ~~are~~ reconstructed from raw data as described in Theory and Figure 2 using MATLAB (Provided by Dr Peter J Lally) and transferred to Python for further processing [12]. For consistency, the Multi-echo FLASH images ~~are~~ also reconstructed from raw data using MATLAB, instead of directly using the default DICOM file from the ~~scanner~~. A mask shown in Figure 5 ~~is~~ extracted from the phantom MR image and used to exclude areas outside the fiducial spheres. The decay time-related images (Multi-echo FLASH), or F-states (ka-SPGR) ~~are~~ masked, and then fitting ~~is~~ performed as shown in Figure 2 to compute T2* values for each pixel. As the range of interest for T2* is around 13ms - 53ms ~~the~~ the phantom spheres with T2* largely outside this range ~~are~~ excluded for further analysis.

The quantitative T2* mapping images using both techniques are generated by colour-coding the T2* values obtained on top of a greyscale averaged image of the multiple acquisitions. ~~It is used to prove the ability to distinguish PD and healthy biomarkers using a quantitative T2*~~ ~~mapping image~~.

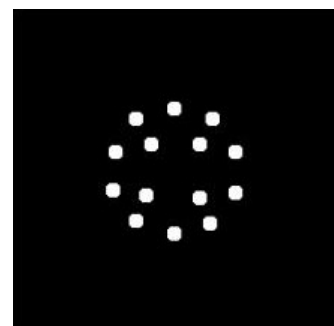


Figure 5: Mask used to extract only fiducial spheres of the Phantom

4.2.3 Analysis method

The T2* percentage error is computed to evaluate the accuracy of ka-SPGR T2* measurement in reality, with the ground truth for each voxel defined by the T2* measured with 90° flip angle Multi-echo FLASH. Taking into account the variation caused by the Gold-standard technique's measurements, a percentage error < 10% would be acceptable in order to detect the change.

The Effective T2* SNR of ka-SPGR and Multi-echo GRE ~~are~~ calculated to compare their efficiency, ~~it can be computed~~ using the equation,

$$T2^*SNR_{effective} = \frac{mean(T2^*)}{\sigma(T2^*) \times \sqrt{t_{effective}}} \quad (4)$$

All factors that affect the efficiency - the effective acquisition time, the number of acquisitions required and the T2* measurement variation are considered in the above equation. Also, to match the ~~environment~~, 20° ~~low~~ flip angle Multi-echo GRE ~~is~~ used for the comparison.

5 Results

The computer simulation and MRI phantom scanning experiment results are presented below.

5.1 Model simulation result

5.1.1 Optimal ka-SPGR parameter

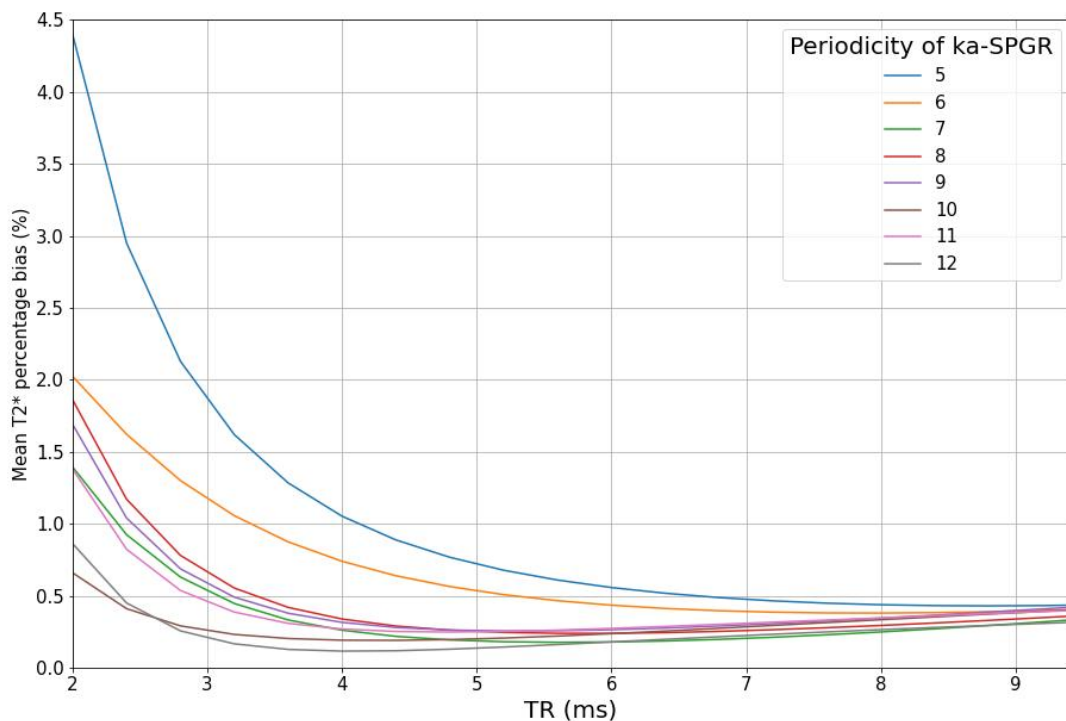


Figure 6: Each line plot shows the changing of the averaged $T2^*$ percentage bias with TR for a specific periodic ka-SPGR sequence, and the plots for 5-12 periodic ka-SPGR are shown in the graph using different colours.

The average $T2^*$ percentage error in the PD biomarker detection range (13-53ms) is calculated for the simulated data of ka-SPGR with periods and TRs listed in Table 1. By plotting the average percentage error against TR for each periodic ka-SPGR as shown in Figure 6, it is found that the smallest bias of 0.1% can be achieved using 12-periodic ka-SPGR with TR = 3.5ms. However, constrained by the minimum 6ms TR that the MRI scanner used in this project can achieve, 7-periodic and 12-periodic ka-SPGR with TR = 6ms are used in the scan.

5.1.2 Optimal ka-SPGR accuracy and precision

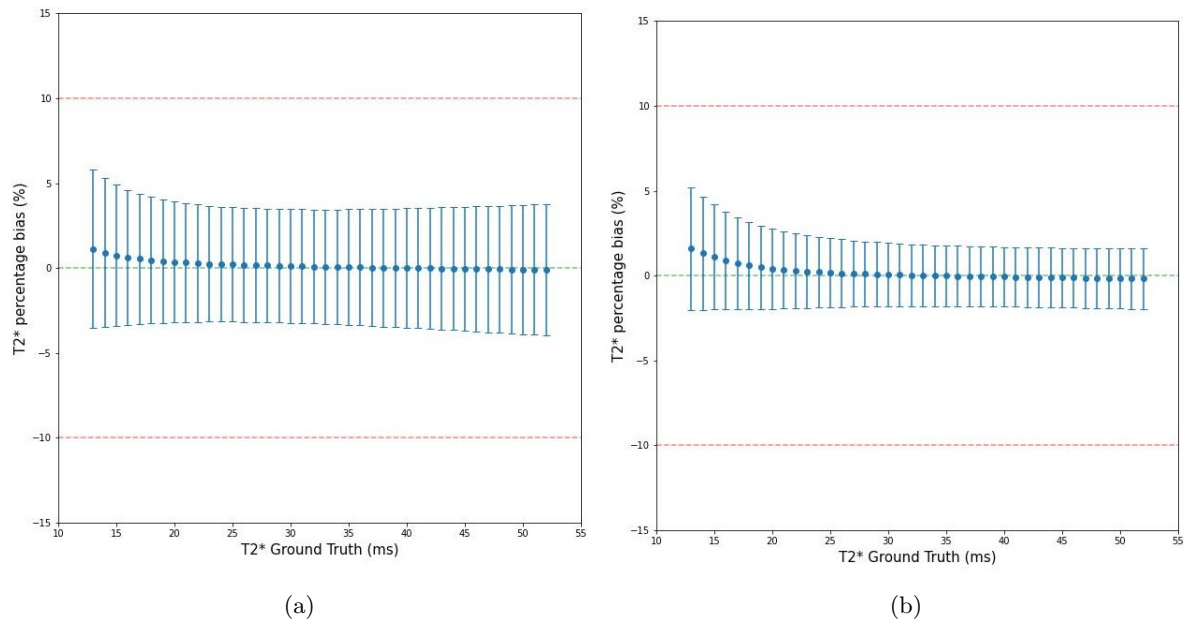


Figure 7: The simulated $T2^*$ percentage bias and the error bar for the 7-periodic (a) and 12-periodic (b) ka-SPGR with TR = 6ms are shown in the plots. A green dotted line shows the zero bias and red dotted lines show $\pm 10\%$ bias.

The Figure 7 shows the bias and variation of the simulated $T2^*$ values at different ground truth values using 7-periodic ka-SPGR (7a) and 12-periodic ka-SPGR (7b). As shown in the graph, for both ka-SPGR sequences the percentage bias approximately lay on the zero-bias line without obvious variations and the error bars are all strictly inside the $\pm 10\%$ bias line. The 2 ka-SPGR sequences have approximately the same percentage bias, however, the 7-periodic ka-SPGR has a two times significantly larger standard deviation than the 12-periodic.

5.2 Phantom MRI scan results

5.2.1 Quantitative $T2^*$ mapping image

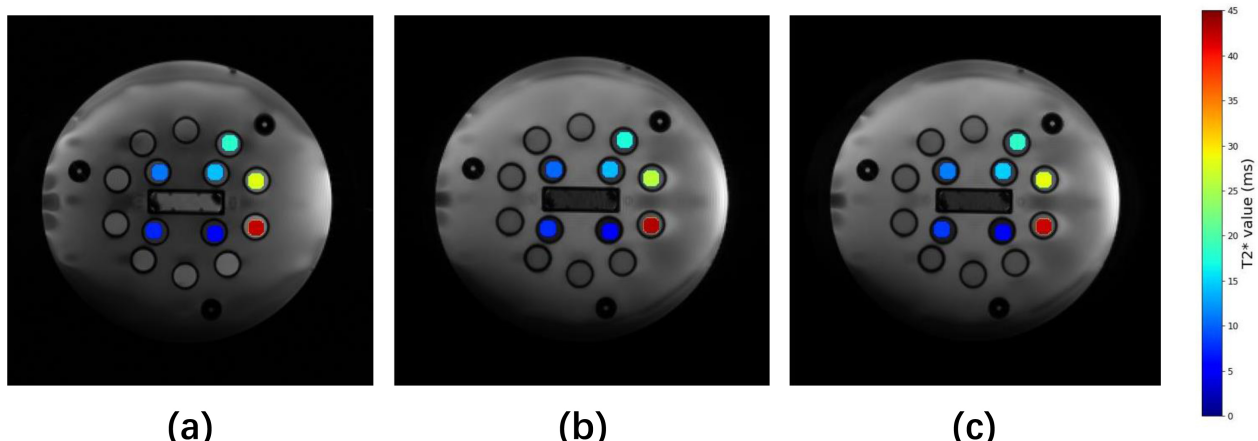
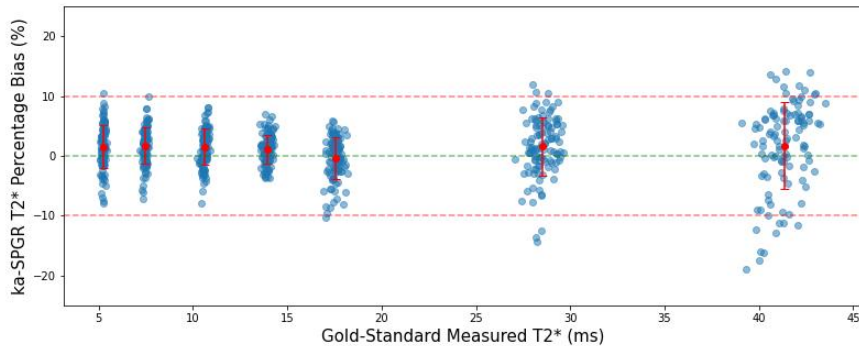


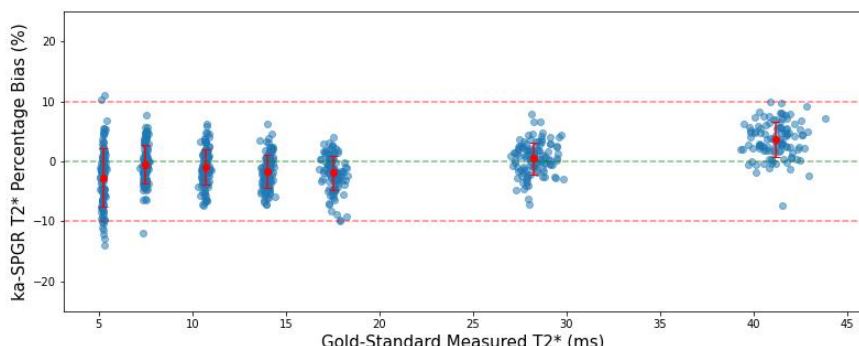
Figure 8: The quantitative $T2^*$ mapping images of the phantom using Gold-standard Multi-echo GRE (a), 7-periodic ka-SPGR (b) and 12-periodic ka-SPGR (c) with the same colourmap. Only the fiducial spheres with PD biomarker-related $T2^*$ are mapped on top of the greyscale image.

As shown in Figure 8, the ~~colours~~ of each fiducial sphere ~~are~~ approximately the same in all 3 T2* mapping images, which shows the ka-SPGR T2* mapping result (Figure 8(b)(c)) aligns with the gold standard (Figure 8(a)). Additionally, there are no large variations of ~~colour~~ in each fiducial sphere.

5.2.2 Percentage bias



(a) 7-periodic ka-SPGR



(b) 12-periodic ka-SPGR

Figure 9: The percentage bias calculated for each voxel is scattered as blue dots, and the mean is plotted in red with an error bar for each fiducial sphere. A horizontal green dotted line is used to show the zero bias, with two red dotted lines showing the $\pm 10\%$ bias.

The T2* percentage bias is computed for each voxel and plotted in Figure 9, each group of points are voxels from the same fiducial sphere and ~~distribute~~ along the x-axis according to the voxel's ground truth T2* value. Each group's mean and standard deviation are calculated and plotted as a red error bar on top of the scattered points. For both 7-periodic and 12-periodic ka-SPGR, the mean bias of each fiducial sphere (red dot) stays within $\pm 5\%$ bias, and all the error bars lay inside $\pm 10\%$ bias for both plots. Additionally, the 12-periodic ka-SPGR has smaller standard deviations compared with the 7-periodic, especially when measuring a higher T2* value.

5.2.3 Effective T2* Signal-to-Noise ratio

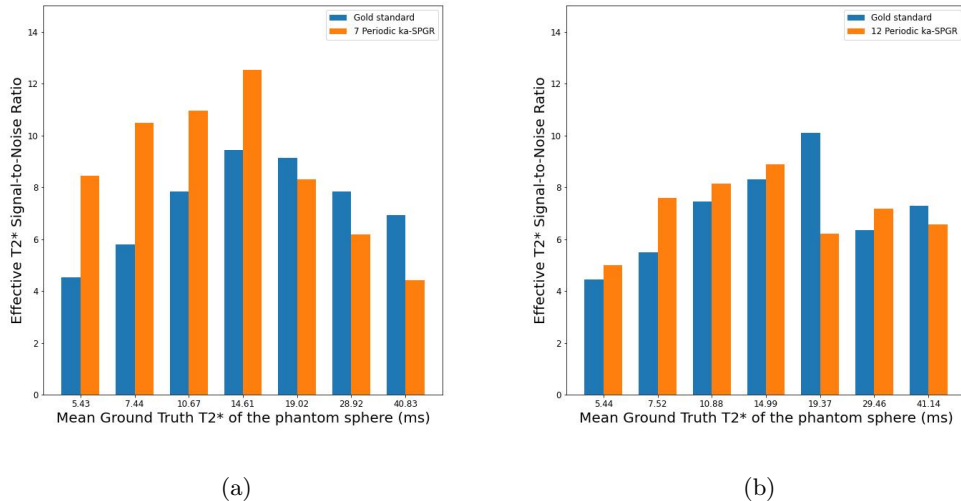


Figure 10: The bar charts show the effective T2* SNR when using the 7-periodic (a)/ 12-periodic (b) ka-SPGR (orange) and the Multi-echo GRE (blue) for each fiducial sphere and the bars are arranged according to increasing T2* order, with the mean ground truth T2* for each sphere labelled on the x-axis.

The effective T2* SNR of 2 optimal ka-SPGR sequences and Multi-echo GRE are compared in the bar chart (Figure 10), and the bars are arranged in increasing T2* order in the x-axis. Both 7-periodic and 12-periodic ka-SPGR have a higher effective T2* SNR than the Multi-echo GRE for measuring a small T2* value of around 5-15ms, notice that the 7-periodic ka-SPGR exhibits a significantly high-efficiency improvement of about 40% at this range. At higher T2* values, both ka-SPGR sequences have similar effective T2* SNR as the Multi-echo GRE, with no improvement observed.

6 Discussion and Conclusion

Result discussion

The optimal 6ms TR 7- and 12-periodic ka-SPGR sequences are both proved to achieve an accurate and precise T_{2*} value measurement with less than $\pm 5\%$ bias by computer simulation and less than $\pm 10\%$ bias by MRI phantom scan results (Figure 7, 9). Compared to previous work on T_{2*} mapping at SN using Multi-echo GRE which has a percentage error of around 8-15%, it supports that the optimised ka-SPGR sequence can be used to detect T_{2*} in the PD biomarker detection range. In Figure 9b, an unexpected significant bias is found for the highest T_{2*} value fiducial spheres, which could be related to the increasing bias and variation of the gold-standard Multi-echo GRE technique. The T_{2*} variation using the Multi-echo GRE can also be observed in the T_{2*} mapping image constructed in previous studies [21].

The T_{2*} mapping images (Figure 8) obtained and the effective T_{2*} SNR (Figure 10) both support the alignment of the ka-SPGR technique result with the gold-standard technique and suggest that it can be considered as an alternative T_{2*} measuring method to the traditional technique. Additionally, the T_{2*} mapping images also show the ability to distinguish PD and healthy SN T_{2*}, which can be identified using blue and red, respectively. As the blue and red coloured fiducial sphere are homogenous and does not have voxels containing extremely out-of-range colour, this shows the measurement variation will not affect the identification of the PD biomarker and ka-SPGR T_{2*} mapping image can be potentially used for PD biomarker detection.

Comparing the optimised ka-SPGR sequences, both simulation and phantom scanning results suggest the 12-periodic is a more precise T_{2*} measurement technique and has more tolerance to noise as its standard deviation is almost halved compared to the 7-periodic (Figure 7, 9). It could be explained by the five additional F-states that 12-periodic can reconstruct compared with 7-periodic, as the region data points cover is more favourable [5], the measurement variation decrease. Besides, Figure 10 suggests the T_{2*} measurement efficiency of 7-periodic ka-SPGR is higher than 12-periodic across the PD biomarker detection range and even about 40% higher than the gold-standard T_{2*} measuring technique for small T_{2*} detection when scanning under matched environment. It indicates the 7-periodic ka-SPGR will be a promising technique for detecting T_{2*} PD biomarkers, given its high efficiency in detecting low T_{2*} values. These choices of parameters are also observed in several previous studies, where 12 echoes [3], 7 echoes [12] and similar 8 echoes [5, 1] are used to acquire T_{2*} value.

Limitations and Possible Improvements

However, the study has the following limitations and can be improved. Firstly, the phantom scanning experiment can't completely represent the ka-SPGR's T_{2*} measurement performance for SN, as the T₁ of the phantom used in this experiment are not specifically aligned with the SN T₁ value. This means the detected signal intensity will be different due to different T₁ and will result in different T_{2*} measurement efficiency for both the ka-SPGR and gold-standard techniques. To perform a more realistic analysis for SN, the phantom sphere should be designed to align with the SN's T₁ and T₂. Secondly, as the T_{2*} ground truth value for the phantom scanning experiment is measured using the Multi-echo GRE sequence, the obtained ground truth T_{2*} value has variation and bias that will affect the analysis. One possible solution is using a phantom specifically designed for T_{2*} mapping with known ground truth T_{2*} values for each fiducial sphere. Last but not least, as the in vivo environment is much more complex than an ideal MRI phantom, the phantom scanning experiment isn't enough to fully support the ka-SPGR's ability for detecting the PD biomarker in vivo. Therefore, in vivo MRI scan experiments should be carried out to analyse ka-SPGR performance in more complex environments and a large number of in vivo tests

would be required to statistically support T2* measurement using ka-SPGR can be used for PD biomarker detection. Furthermore, the optimal parameters suggested in this study can be extended to perform in vivo experiments for exploring the motion robustness of the ka-SPGR, which is potentially a huge advantage compared with other existing techniques.

Conclusion

This study has found that using a 7- or 12-periodic ka-SPGR sequence with TR = 6ms can achieve acceptable accurate and precise measurement of T2 in the PD biomarker detection range. To perform a more efficient scan, 7-periodic ka-SPGR is more favourable and will be able to detect the PD-related T2* drop effectively. With no time limitation, 12-period will be a better choice as it is more robust to noise. However, an MRI phantom designed using SN tissue property with known T2* is highly desirable to perform a more accurate analysis of ka-SPGR T2* mapping performance and further in vivo experiments are essential to support the optimised ka-SPGR's ability to detect PD biomarker.

7 Acknowledgements

References

- [1] Simon Baudrexel, Lucas Nürnberger, Udo Rüb, Carola Seifried, Johannes C. Klein, Thomas Deller, Helmuth Steinmetz, Ralf Deichmann, and Rüdiger Hilker. Quantitative mapping of t1 and t2 discloses nigral and brainstem pathology in early parkinson's disease. *NeuroImage*, 51:512–520, 2010.
- [2] Daniela Berg, Wolfgang Roggendorf, Ute Schröder, Rüdiger Klein, Thomas Tatschner, Peter Benz, Oliver Tucha, Michael Preier, Klaus W. Lange, Karlheinz Reiners, Manfred Gerlach, and Georg Becker. Echogenicity of the Substantia Nigra: Association With Increased Iron Content and Marker for Susceptibility to Nigrostriatal Injury. *Archives of Neurology*, 59(6):999–1005, 06 2002.
- [3] Malte Brammerloh, Markus Morawski, Isabel Friedrich, Tilo Reinert, Charlotte Lange, Primož Pelicon, Primož Vavpetič, Steffen Jankuhn, Carsten Jäger, Anneke Alkemade, and et al. Measuring the iron content of dopaminergic neurons in substantia nigra with mri relaxometry. *NeuroImage*, 239:118255, Oct 2021.
- [4] Govind B. Chavhan, Paul S. Babyn, Bejoy Thomas, Manohar M. Shroff, and E. Mark Haacke. Principles, techniques, and applications of t2*-based mr imaging and its special applications. *Radiographics*, 29:1433–1449, 9 2009.
- [5] Hai Ling Margaret Cheng, Nikola Stikov, Nilesh R. Ghugre, and Graham A. Wright. Practical medical applications of quantitative mr relaxometry. *Journal of Magnetic Resonance Imaging*, 36:805–824, 10 2012.
- [6] D. T. Dexter, F. R. Wells, A. J. Lee, F. Agid, Y. Agid, P. Jenner, and C. D. Marsden. Increased nigral iron content and alterations in other metal ions occurring in brain in parkinson's disease. *Journal of Neurochemistry*, 52:1830–1836, 1989.
- [7] Jeff H. Duyn. Steady state effects in fast gradient echo magnetic resonance imaging. *Magnetic Resonance in Medicine*, 37:559–568, 1997.
- [8] Richard R. Ernst, Geoffrey Bodenhausen, and Alexander Wokaun. *Principles of Nuclear Magnetic Resonance in one and two dimensions*. Clarendon Press, 2004.
- [9] Carl Ganter. Steady state of echo-shifted sequences with radiofrequency phase cycling. *Magnetic Resonance in Medicine*, 56:923–926, 2006.
- [10] HáKon Gudbjartsson and Samuel Patz. The rician distribution of noisy mri data. *Magnetic Resonance in Medicine*, 34:910–914, 1995.
- [11] Samantha J. Holdsworth, Mahdi Salmani Rahimi, Wendy W. Ni, Greg Zaharchuk, and Michael E. Moseley. Amplified magnetic resonance imaging (amri). *Magnetic Resonance in Medicine*, 75:2245–2254, 6 2016.
- [12] Peter J Lally, Mark Chiew, Paul M Matthews, Karla L Miller, and Neal K Bangerter. A motion-robust, short-tr alternative to multi-echo spgr.
- [13] Christian Langkammer, Nikolaus Krebs, Walter Goessler, Eva Scheurer, Franz Ebner, Kathrin Yen, Franz Fazekas, and Stefan Ropele. Quantitative mr imaging of brain iron: A postmortem validation study. *Radiology*, 257(2):455–462, Nov 2010.
- [14] Sen Ma, Nan Wang, Yibin Xie, Zhaoyang Fan, Debiao Li, and Anthony G. Christodoulou. Motion-robust quantitative multiparametric brain mri with motion-resolved mr multitasking. *Magnetic Resonance in Medicine*, 87:102–119, 1 2022.
- [15] W. R. Wayne Martin, Marguerite Wieler, and Myrlene Gee. Midbrain iron content in early parkinson disease. *Neurology*, 70(16 Part 2):1411–1417, 2008.

- [16] N. Maserejian, L. Vinikoor-Imler, and A. Dilley. Estimation of the 2020 global population of parkinson's disease (pd)[abstract]. *mov disord.* 2020; 35 (suppl 1).
- [17] Ricarda A. Menke, Jan Scholz, Karla L. Miller, Sean Deoni, Saad Jbabdi, Paul M. Matthews, and Mojtaba Zarei. Mri characteristics of the substantia nigra in parkinson's disease: A combined quantitative t1 and dti study. *NeuroImage*, 47:435–441, 8 2009.
- [18] Dwight G. Nishimura. *Principles of Magnetic Resonance Imaging*. Lulu.com, 2010.
- [19] Werner Poewe, Klaus Seppi, Caroline M. Tanner, Glenda M. Halliday, Patrik Brundin, Jens Volkmann, Anette Eleonore Schrag, and Anthony E. Lang. Parkinson disease. *Nature Reviews Disease Primers*, 3:1–21, 3 2017.
- [20] Stefan Theodor Schwarz, Olivier Mougin, Yue Xing, Anna Blazejewska, Nin Bajaj, Dorothee P. Auer, and Penny Gowland. Parkinson's disease related signal change in the nigrosomes 1–5 and the substantia nigra using t2* weighted 7t mri. *NeuroImage: Clinical*, 19:683–689, 1 2018.
- [21] Seonyeong Shin, Seong Dae Yun, and N. Jon Shah. T2* quantification using multi-echo gradient echo sequences: a comparative study of different readout gradients. *Scientific Reports*, 13, 12 2023.
- [22] Matthias Weigel. Extended phase graphs: Dephasing, rf pulses, and echoes - pure and simple. *Journal of Magnetic Resonance Imaging*, 41:266–295, 2 2015.
- [23] Dmitriy A. Yablonskiy and E. Mark Haacke. Theory of nmr signal behavior in magnetically inhomogeneous tissues: The static dephasing regime. *Magnetic Resonance in Medicine*, 32:749–763, 1994.